Nonlinear vibration of unsymmetric double-layer lattice truss core sandwich beams

Na Hao[a], Linfeng Zhu[a], Zhangming Wu[b,c], Liaoliang Ke[a,*]

[a] *School of Mechanical Engineering, Tianjin University, Tianjin, 300350, China*

[b] *School of Mechanical Engineering and Mechanics, Ningbo University, Ningbo, 315211, China*

[c] *School of Engineering, Cardiff University, Cardiff CF24 3AA, UK*

Abstract

In recent years, many novel sandwich structures with multilayer or graded lattice truss cores that exhibited superior structural performance have been proposed. However, only limited works have studied the nonlinear behavior of sandwich structures with unsymmetric lattice truss cores. This paper aims to provide an analytical study on the nonlinear vibration of the unsymmetric double-layer lattice truss core sandwich beams (LTCSBs). The double-layer LTCSB is designed to be unsymmetric and possess varying material property and structural geometry in each layer. In this study, six unsymmetric cases of LTCSB classified as two categories according to the midplane locations are considered. Subsequently, an analytical model for the unsymmetric double-layer LTCSB is developed based on the Allen's model and von Kármán nonlinear theory. The axial displacement of the midplane of LTCSB is considered in the analytical model, therefore the proposed model is more generalized compared with previous models for the symmetric double-layer LTCSB. The Ritz method with a direct iterative procedure is applied to solve the nonlinear governing equations and determine the nonlinear frequencies for the unsymmetric double-layer LTCSB. Finally, the effects of six unsymmetric cases of LTCSBs on the nonlinear frequency ratio versus amplitude curve under three different types of boundary conditions is discussed detailly. An interesting phenomenon of softening-spring nonlinearity is found for hinged-hinged and clamped-hinged sandwich beams with large bending-extension coupling.

Keywords: Nonlinear vibration, Sandwich beams, Lattice truss core, Softening-spring nonlinearity

* Corresponding author. E-mail: llke@tju.edu.cn (L.L. Ke).

1. Introduction

Sandwich structures have been widely applied in many engineering fields. In recent years, cellular materials manufactured by advanced 3D printing technologies attract increasingly attentions due to their high stiffness and strength yet lightweight properties [1-3]. Previous research works have demonstrated that some newly developed lattice sandwich structures with three-dimensional truss cores exhibit prominent mechanical properties [4-7]. For example, lightweight multilayered graded lattice sandwich structures are designed to achieve superior impact resistance and energy absorption capacities for engineering applications [8, 9]. Increasing number of researchers are dedicated to developing advanced manufacturing technologies [10-14] and design methods [15-20] for lattice truss core sandwich structures, which will have wide applications in architectures, ships, high-speed trains, biomedical devices, aerospace, and many other engineering fields.

Structural vibration problems are commonly existed in many engineering fields, which often accelerate the damaging process of the structures. The vibration problem of sandwich structures with a single-layer lattice truss core had been well studied in previous works using theoretical, experimental, and numerical methods [21-25]. Based on Allen's model [26], Lou et al. [27] analyzed the linear vibration characteristics of sandwich beams with pyramidal truss cores. Xu and Qiu [28] obtained the natural frequency of composite sandwich beams with pyramidal and tetrahedral truss cores by a combined use of the Euler beam theory and Timoshenko beam theory. Zhao et al. [29] applied the assumed mode method and Hamilton's principle to investigate the vibration of multi-span metal sandwich beams with Kagome and Pyramidal truss cores. However, up to now, only limited research works have been reported to study the nonlinear analysis of lattice truss core sandwich structures [30, 31]. Chai et al. [32] studied the nonlinear vibration behaviour and active control methods for the sandwich plates with a single-layer lattice. Nampally et al. [33] developed a novel nonlinear finite element model to study the nonlinear bending and linear free vibration of single-layer sandwich panels with a pyramid core.

In recent years, sandwich structures with multilayer or graded lattice truss cores were studied and their mechanical behaviors were analyzed [34-39]. Li et al. [40] performed the linear vibration analysis of multilayer LTCSBs with simply supported boundary conditions using theoretical, numerical, and experimental methods. They also developed the novel deformation relations of symmetric multilayer sandwich beams with the lattice truss core in theory. Guo et al. [41] investigated the effect of structural and material parameters on the vibration control of double-layer hourglass sandwich beams using

improved theory method and finite element method (FEM). However, to the best of authors' knowledge, there are no research works that had studied the nonlinear problems of sandwich structures with multilayer or graded lattice truss cores.

In this paper, we study the nonlinear vibration behavior of double-layer LTCSBs that are designed to be unsymmetric about the midplane and have varying material property or structural geometry in each layer. Six unsymmetric cases for double-layer LTCSB are considered and classified as two categories according to the midplane location of the structure. Then, an analytical model based on Allen's model and von Kármán nonlinear theory is developed for the unsymmetric double-layer LTCSBs. Unlike the model developed by Li et al. [40] for symmetric LTCSB, it is not appropriate to directly assume that the midplane is coincident with neutral plane for the unsymmetric LTCSBs when establishing the analytical model with respect to the midplane coordinate. Therefore, the axial displacement of the midplane is considered in this model to capture the nonlinear behavior of unsymmetric double-layer LTCSBs, accurately. Ritz method is applied to determine the linear and nonlinear vibration frequencies of the double-layer LTCSB under different boundary conditions. The analytical model is validated with the numerical results obtained by FEM. Finally, a parametric study is carried out to investigate the effects of material properties, geometry structures and boundary conditions on the nonlinear dynamic behavior of the double-layer LTCSB.

2. Description of unsymmetric double-layer LTCSB

Fig. 1 shows the sketch of an unsymmetric double-layer LTCSB with different unit cells in the top and bottom cores. This double-layer LTCSB is composed of top face sheet, mid-sheet, bottom face sheet, top and bottom cores. Three different unit cells in the cores, i.e., the pyramidal, Kagome, and hourglass unit cells are considered. L and H are the length and total thickness of the double-layer LTCSB, respectively; h_{es} and $h_{qc}\left(e=t,b,m,q=t,b\right)$ are the thicknesses of sheets and cores, respectively; h_c, b_c and d_c are the height, width and length of the unit cell, respectively; r_c, L_c and α are the radius, length and inclination angle of struts, respectively. Note, the subscripts t, b, m, s and c, represent 'top', 'bottom', 'middle', 'sheet' and 'core', respectively. The total thickness H of the double-layer LTCSB is the sum of the thicknesses of all the sheets and cores, i.e., $H=h_t+h_{ct}+h_m+h_{cb}+h_b$.

The unsymmetric features of double-layer LTCSBs with respect to the midplane are attributed to the

different material property or structural geometry of each layer. As shown in Fig. 2, six different cases for double-layer LTCSBs are considered in the present paper:

Case I: The materials in two layers are different, bottom core and sheet are made of material 1 (Al_2O_3) and the rest part is made of material 2 (ZrO_2 or aluminum (Al)).

Case II: The thicknesses of top and bottom face sheets are different ($h_{bs} > h_{ts}$, and h_{bs} / h_{ts} is variable).

Case III: The thicknesses of top and bottom cores are different ($h_{bc} > h_{tc}$, $h_{bc} + h_{tc}$ is constant while h_{bc} / h_{tc} is variable).

Case IV: The lengths of unit cells in top and bottom cores are different ($d_{bc} \neq d_{tc}$ and d_{bc} / d_{tc} is variable).

Case V: The struts radii of unit cells in top and bottom cores are different ($r_{bc} \neq r_{tc}$ and r_{bc} / r_{tc} is variable).

Case VI: The types of unit cells in top and bottom cores are different, the unit cell in bottom core is cell 1 (pyramidal cell) and the top core is consistent with the unit cell 2 (Kagome or hourglass unit cell).

Except the differences that are listed in Table. 1 for cases I-VI, other parameters are the same for these two layers. Note, only pyramidal unit cell is applied in cases I-V and only Al_2O_3 is applied in cases II-VI.

In the theoretical analysis, the lattice truss core is assumed as an equivalent layer of continuum [28]. Consequently, the equivalent density and the transverse shear modulus of the lattice truss core are expressed as [42]

$$\rho_c = \rho \cdot \bar{\rho}\,, \tag{1}$$

$$G_c = \frac{E \cdot \bar{\rho} \cdot \sin^2(2\alpha)}{8}, \tag{2}$$

where ρ and E are the mass density and elastic modulus of base material, respectively; $\bar{\rho}$ denotes the relative density of the truss core, which is the ratio between the struts volume and the unit cell volume. For pyramidal, Kagome and hourglass truss cores, the relative densities are derived as [32, 43]

$$\bar{\rho}^{pyr} = \frac{2\pi r_c^{\,2}}{L_c^{\,2}\cos^2(\alpha)\sin(\alpha)}, \tag{3}$$

$$\bar{\rho}^{Kag} = \frac{3\pi r_c^{\,2}}{2L_c^{\,2}\cos^2(\alpha)\sin(\alpha)}, \tag{4}$$

$$\bar{\rho}^{hou} = \frac{4\pi r_c^{\,2}}{L_c^{\,2}\cos^2(\alpha)\sin(\alpha)}, \tag{5}$$

where α is the inclination angle for different cases and is determined by the geometric relations of a unit cell.

3. Formulations of nonlinear vibration problem

When studying the lattice truss core sandwich structures, the following assumptions are applied generally [27]: (i) three sheets are modelled as Euler beams; (ii) transverse shear deformation in two core layers is considered; (iii) the sheets and the core layers have the same transverse displacements but different axial displacements and rotation angles; (iv) there is no slippage or movement between the interfaces.

3.1 Energy functional

Fig. 3 illustrates undeformed and deformed states of an infinitesimal element of the unsymmetric double-layer LTCSB. The displacements fields of double-layer LTCSBs for Fig. 3(a) and Fig. 3(b) are defined with respect to the midplane coordinate. For cases II and III, the midplane lies in the bottom core layer as shown in Fig. 3(a), while for cases I and IV-VI the midplane lies in the middle position of the middle sheet as shown in Fig. 3(b). According to the deformation relationships as illustrated in Fig. 3, the axial displacements of various points on the deformed infinitesimal element in Fig. 3(a) are given

$$u_{ts} = u\left(x,t\right) - H_0\theta - \left(z - H_0\right)\frac{\partial w}{\partial x},\ \frac{H}{2} - h_{ts} \le z \le \frac{H}{2}, \tag{6}$$

$$u_{tc} = u\left(x,t\right) - h_{ms}\frac{\partial w}{\partial x} - \left(z - h_{ms}\right)\theta,\ H_1 + h_{ms} \le z \le \frac{H}{2} - h_{ts}, \tag{7}$$

$$u_{ms} = u\left(x,t\right) - H_1\theta - \left(z - H_1\right)\frac{\partial w}{\partial x},\ \ H_1 \le z \le H_1 + h_{ms}, \tag{8}$$

$$u_{bc} = u\left(x,t\right) - z\theta,\ \ -H_2 \le z \le H_1, \tag{9}$$

$$u_{bs} = u\left(x,t\right) + H_2\theta - \left(z + H_2\right)\frac{\partial w}{\partial x},\ -\frac{H}{2} \le z \le -H_2, \tag{10}$$

where $H_0 = H_1 + h_{tc}$, $H_1 = H/2 - h_{ts} - h_{tc} - h_{ms}$ and $-H_2 = -H/2 + h_{bs}$ are z-axis coordinates; u and w are the displacement components in the midplane; θ and $\partial w/\partial x$ are the rotations of the lattice truss core and three sheets, respectively. u_{es} and u_{qc} represent the axial displacement in sheets and cores, respectively. Similarly, the displacements fields of Fig. 3(b) are expressed as

$$u_{ts} = u\left(x,t\right) - h_c\theta - \left(z - h_c\right)\frac{\partial w}{\partial x},\ \frac{H}{2} - h \le z \le \frac{H}{2}, \tag{11}$$

$$u_{tc} = u\left(x,t\right) - \frac{h}{2}\frac{\partial w}{\partial x} - \left(z - \frac{h}{2}\right)\theta,\ \frac{h}{2} \le z \le \frac{h}{2} + h_c, \tag{12}$$

$$u_{ms} = u\left(x,t\right) - z\frac{\partial w}{\partial x},\ -\frac{h}{2} \le z \le \frac{h}{2}, \tag{13}$$

$$u_{bc} = u(x,t) + \frac{h}{2}\frac{\partial w}{\partial x} - \left(z + \frac{h}{2}\right)\theta,\ -\frac{h}{2} - h_c \le z \le -\frac{h}{2}, \tag{14}$$

$$u_{bs} = u(x,t) + h_c\theta - (z + h_c)\frac{\partial w}{\partial x},\ -\frac{H}{2} \le z \le -h_c - \frac{h}{2}, \tag{15}$$

where h_c $\left(h_c = h_{tc} = h_{bc}\right)$ and h $\left(h = h_{ts} = h_{bs} = h_{ms}\right)$ are the thicknesses of the two cores and three sheets, respectively. In this analysis, the midplane of unsymmetric double-layer LTCSBs is likely to have an axial displacement, i.e., the midplane and neutral plane do not coincide. This assumption on the midplane of unsymmetric sandwich beams is different from other theoretical models [25, 40, 41].

With the von Kármán nonlinear geometric approximation, the strain-displacement relations of sheets and core layers of the LTCSB are defined as

$$\varepsilon_{es} = \frac{\partial u_{es}}{\partial x} + \frac{1}{2}\left(\frac{\partial w}{\partial x}\right)^2, \tag{16}$$

$$\gamma_{qc} = \frac{\partial w}{\partial x} - \theta, \tag{17}$$

where ε_{es} and γ_{qc} are the normal strain and shear strain, respectively.

The normal and shear stresses are given by the elastic constitutive law

$$\sigma_{es} = E_{es}\varepsilon_{es},\ \tau_{qc} = G_{qc}\gamma_{qc}. \tag{18}$$

Substituting Eqs. (16) and (17) into Eq. (18), the corresponding stresses σ_{ts}, σ_{ms}, σ_{bs}, τ_{tc} and τ_{bc} are computed. Consequently, the force and bending moment resultants of the unsymmetric double-layer LTCSB are

$$N_x = B\left(\int \sigma_{ts}\mathrm{d}z + \int \sigma_{ms}\mathrm{d}z + \int \sigma_{bs}\mathrm{d}z\right), \tag{19}$$

$$M_x = B\left(\int z\sigma_{ts}\mathrm{d}z + \int z\sigma_{ms}\mathrm{d}z + \int z\sigma_{bs}\mathrm{d}z\right), \tag{20}$$

where *B* is the width of double-layer LTCSB. Note, the ranges of integration in Eqs. (19) and (20) are different for different unsymmetric cases.

Taking Fig. 3(a) as an example, the midplane is located at the bottom core layer. Then, the strain energy *Q* and kinetic energy *J* are expressed as [44]

$$Q = \frac{B}{2}\int_0^L \left\{ \int_{\frac{H}{2}-h_{ts}}^{\frac{H}{2}} \sigma_{ts}\varepsilon_{ts}\mathrm{d}z + \int_{H_1+h_{ms}}^{\frac{H}{2}-h_{ts}} \tau_{tc}\gamma_{tc}\mathrm{d}z + \int_{H_1}^{H_1+h_{ms}} \sigma_{ms}\varepsilon_{ms}\mathrm{d}z + \int_{-H_2}^{H_1} \tau_{bc}\gamma_{bc}\mathrm{d}z + \int_{-\frac{H}{2}}^{-H_2} \sigma_{bs}\varepsilon_{bs}\mathrm{d}z \right\}\mathrm{d}x, \tag{21}$$

$$J=\frac{B}{2}\int_0^L\left\{\int_{\frac{H}{2}-h_{ts}}^{\frac{H}{2}}\rho_{ts}\left[\left(\frac{\partial u_{ts}}{\partial t}\right)^2+\left(\frac{\partial w}{\partial t}\right)^2\right]\mathrm{d}z+\int_{H_1+h_{ms}}^{\frac{H}{2}-h_{ts}}\rho_{tc}\left[\left(\frac{\partial u_{tc}}{\partial t}\right)^2+\left(\frac{\partial w}{\partial t}\right)^2\right]\mathrm{d}z\right.$$
$$+\int_{H_1}^{H_1+h_{ms}}\rho_{ms}\left[\left(\frac{\partial u_{ms}}{\partial t}\right)^2+\left(\frac{\partial w}{\partial t}\right)^2\right]\mathrm{d}z+\int_{-H_2}^{H_1}\rho_{bc}\left[\left(\frac{\partial u_{bc}}{\partial t}\right)^2+\left(\frac{\partial w}{\partial t}\right)^2\right]\mathrm{d}z \quad . \tag{22}$$
$$\left.+\int_{-\frac{H}{2}}^{-H_2}\rho_{bs}\left[\left(\frac{\partial u_{bs}}{\partial t}\right)^2+\left(\frac{\partial w}{\partial t}\right)^2\right]\mathrm{d}z\right\}\mathrm{d}x$$

Substituting Eqs. (6)-(10) and Eq. (18) into Eqs. (19)-(22), the maximum potential energy $Q_{\max}$ ($Q_{\max}=Q_{linear}+Q_{nonlinear}$), kinetic energy $J_{\max}$, force and bending moment resultants are given by

$$Q_{linear}=\frac{B}{2}\int_0^L\left\{A_{11}\left(\frac{\partial u}{\partial x}\right)^2+A_{13}\left(\frac{\partial\theta}{\partial x}\right)^2+\left(D_{11}+A_{13}-2B_{12}\right)\left(\frac{\partial^2 w}{\partial x^2}\right)^2-2A_{12}\frac{\partial u}{\partial x}\frac{\partial\theta}{\partial x}\right.$$
$$\left.-2\left(B_{11}-A_{12}\right)\frac{\partial u}{\partial x}\frac{\partial^2 w}{\partial x^2}+A_{00}\left[\left(\frac{\partial w}{\partial x}\right)^2-2\theta\frac{\partial w}{\partial x}+\theta^2\right]+2\left(B_{12}-A_{13}\right)\frac{\partial\theta}{\partial x}\frac{\partial^2 w}{\partial x^2}\right\}\mathrm{d}x \tag{23}$$

$$Q_{nonlinear}=\frac{B}{2}\int_0^L\left\{\frac{A_{11}}{4}\left(\frac{\partial w}{\partial x}\right)^4+A_{11}\frac{\partial u}{\partial x}\left(\frac{\partial w}{\partial x}\right)^2-A_{12}\frac{\partial\theta}{\partial x}\left(\frac{\partial w}{\partial x}\right)^2-\left(B_{11}-A_{12}\right)\left(\frac{\partial w}{\partial x}\right)^2\frac{\partial^2 w}{\partial x^2}\right\}\mathrm{d}x, \tag{24}$$

$$J_{\max}=\frac{\Omega^2 B}{2}\int_0^L\left\{L_{11}u^2+\left(L_{12}-2L_{24}+L_{31}\right)\theta^2+\left(L_{12}-2L_{22}+L_{32}\right)\left(\frac{\partial w}{\partial x}\right)^2+2\left(L_{13}-L_{21}\right)u\frac{\partial w}{\partial x}\right.$$
$$\left.+L_{11}w^2-2\left(L_{13}+L_{23}\right)u\theta+2\left(L_{25}-L_{12}\right)\theta\frac{\partial w}{\partial x}\right\}\mathrm{d}x \tag{25}$$

$$N_x=A_{11}\left[\frac{\partial u}{\partial x}+\frac{1}{2}\left(\frac{\partial w}{\partial x}\right)^2\right]-A_{12}\frac{\partial\theta}{\partial x}+\left(A_{12}-B_{11}\right)\frac{\partial^2 w}{\partial x^2}, \tag{26}$$

$$M_x=B_{11}\left[\frac{\partial u}{\partial x}+\frac{1}{2}\left(\frac{\partial w}{\partial x}\right)^2\right]-B_{12}\frac{\partial\theta}{\partial x}+\left(B_{12}-D_{11}\right)\frac{\partial^2 w}{\partial x^2}, \tag{27}$$

where

$$A_{00}=S_{tc}+S_{bc};\ A_{11}=A_{ts}+A_{ms}+A_{bs},\ A_{12}=H_0A_{ts}+H_1A_{ms}-H_2A_{bs},$$

$$\mathrm{A}_{13}=H_0{}^2A_{ts}+H_1{}^2A_{ms}+H_2{}^2A_{bs};$$

$$B_{11}=B_{ts}+B_{ms}+B_{bs},\ B_{12}=H_0B_{ts}+H_1B_{ms}-H_2B_{bs};\ D_{11}=D_{ts}+D_{ms}+D_{bs};$$

$$L_{11}=I_{ts}^0+I_{tc}^0+I_{bc}^0+I_{ms}^0+I_{bs}^0,\ L_{12}=H_0{}^2I_{ts}^0+h_{ms}{}^2I_{tc}^0+H_1{}^2I_{ms}^0+H_2{}^2I_{bs}^0,$$

$$L_{13}=H_0I_{ts}^0-h_{ms}I_{tc}^0+H_1I_{ms}^0-H_2I_{bs}^0;$$

$$L_{21}=I_{ts}^{1}+I_{ms}^{1}+I_{bs}^{1},\ L_{22}=H_0I_{ts}^{1}+H_1I_{ms}^{1}-H_2I_{bs}^{1},\ L_{23}=I_{tc}^{1}+I_{bc}^{1},\ L_{24}=h_{ms}I_{tc}^{1},$$

$$L_{25}=H_0I_{ts}^{1}+H_1I_{ms}^{1}+h_{ms}I_{tc}^{1}-H_2I_{bs}^{1};$$

$$L_{31}=I_{tc}^{2}+I_{bc}^{2},\ L_{32}=I_{ts}^{2}+I_{ms}^{2}+I_{bs}^{2}.$$

The unknown terms in L_{11}-L_{32}, A_{00}, A_{11}, A_{12}, A_{13}, B_{11}, B_{12} and D_{11} are expressed as [45]

$$\begin{aligned}
&\left(A_{ts},B_{ts},D_{ts}\right)=\int_{\frac{H}{2}-h_{ts}}^{\frac{H}{2}}E_{ts}\left(1,z,z^2\right)\mathrm{d}z,\ \left(A_{ms},B_{ms},D_{ms}\right)=\int_{H_1}^{H_1+h_{ms}}E_{ms}\left(1,z,z^2\right)\mathrm{d}z,\\
&\left(A_{bs},B_{ts},D_{bs}\right)=\int_{-\frac{H}{2}}^{-H_2}E_{bs}\left(1,z,z^2\right)\mathrm{d}z,\ \ S_{tc}=\int_{H_1+h_{ms}}^{\frac{H}{2}-h_{ts}}G_{tc}\mathrm{d}z,S_{bc}=\int_{-H_2}^{H_1}G_{bc}\mathrm{d}z,\\
&I_{ts}^{i}=\int_{\frac{H}{2}-h_{ts}}^{\frac{H}{2}}\rho_{ts}z^{i}\mathrm{d}z,\ I_{ms}^{i}=\int_{H_1}^{H_1+h_{ms}}\rho_{ms}z^{i}\mathrm{d}z,I_{bs}^{i}=\int_{-\frac{H}{2}}^{-H_2}\rho_{bs}z^{i}\mathrm{d}z,\\
&I_{tc}^{i}=\int_{H_1+h_{ms}}^{\frac{H}{2}-h_{ts}}\rho_{tc}z^{i}\mathrm{d}z,I_{bc}^{i}=\int_{-H_2}^{H_1}\rho_{bc}z^{i}\mathrm{d}z,
\end{aligned}\tag{28}$$

where $i=0,1,2$. The coefficients B_{11} is recognized as the main contribution to the bending-extension coupling effect for the unsymmetric double-layer LTCSB.

The following dimensionless quantities are introduced:

$$\begin{aligned}
&\xi=\frac{x}{L},\ \left(U,W\right)=\frac{\left(u,w\right)}{H},\ \varphi=\theta,\ A_{10}=\int_{-\frac{H}{2}}^{\frac{H}{2}}E_{bs}\mathrm{d}z,\ I_{10}=\int_{-\frac{H}{2}}^{\frac{H}{2}}\rho_{bs}\mathrm{d}z,\\
&\omega=\Omega L\sqrt{I_{10}/A_{10}},\ \zeta_1=\frac{h_{ms}}{H},\ \zeta_2=\frac{H}{L},\zeta_3=\frac{H_0}{H},\ \zeta_4=\frac{H_1}{H},\ \zeta_5=\frac{H_2}{H},\\
&\left(\bar{A}_{es},\bar{B}_{es},\bar{D}_{es}\right)=\frac{\left(A_{es},B_{es},D_{es}\right)}{A_{10}\left(1,H,H^2\right)},\ \bar{I}_{es}^{i}=\frac{I_{es}^{i}}{I_{10}H^{i}},\bar{I}_{qc}^{i}=\frac{I_{qc}^{i}}{I_{10}H^{i}},\bar{S}_{qc}=\frac{S_{qc}}{A_{10}},\\
&Q^{*}_{linear}=\frac{Q_{linear}}{\Delta_0},\ Q^{*}_{nonlinear}=\frac{Q_{nonlinear}}{\Delta_0},\ J^{*}_{\max}=\frac{J_{\max}}{\Delta_0},\ \Delta_0=\frac{BA_{10}H^2}{L}.
\end{aligned}\tag{29}$$

After applying the dimensionless forms for Eqs. (23)-(25), the following energy functional of the unsymmetric double-layer LTCSB is arrived as

$$\Pi=Q^{*}_{linear}+Q^{*}_{nonlinear}-J^{*}_{\max}.\tag{30}$$

3.2 Ritz method

The governing equations for the nonlinear vibration of the double-layer LTCSB is derived using the Ritz method [46]. Three different boundary conditions, i.e., hinged-hinged (H-H), clamped-clamped (C-C), clamped-hinged (C-H) are considered in the model. The corresponding trial functions are given as [47]:

H-H:
$$\begin{cases} U(\xi)=\sum_{j=1}^{N} A_j \xi^j (1-\xi), \\ W(\xi)=\sum_{j=1}^{N} B_j \xi^j (1-\xi), \\ \varphi(\xi)=\sum_{j=1}^{N} C_j \xi^{j-1}, \end{cases} \tag{31}$$

C-C:
$$\begin{cases} U(\xi)=\sum_{j=1}^{N} A_j \xi^j (1-\xi), \\ W(\xi)=\sum_{j=1}^{N} B_j \xi^j (1-\xi), \\ \varphi(\xi)=\sum_{j=1}^{N} C_j \xi^j (1-\xi), \end{cases} \tag{32}$$

C-H:
$$\begin{cases} U(\xi)=\sum_{j=1}^{N} A_j \xi^j (1-\xi), \\ W(\xi)=\sum_{j=1}^{N} B_j \xi^j (1-\xi), \\ \varphi(\xi)=\sum_{j=1}^{N} C_j \xi^j, \end{cases} \tag{33}$$

where N is the number of the polynomial terms; A_j, B_j and C_j are unknown coefficients. Substituting one of Eqs. (31)-(33) into Eq. (30) and minimizing the total energy with respect to unknown coefficients yield:

$$\frac{\partial \Pi}{\partial A_j}=0,\ \frac{\partial \Pi}{\partial B_j}=0,\ \frac{\partial \Pi}{\partial C_j}=0. \tag{34}$$

Consequently, the nonlinear governing equations are expressed in a matrix form as

$$\left(\left[\mathbf{K_L}\right]+\left[\mathbf{K_{NL1}}\right]+\left[\mathbf{K_{NL2}}\right]\right)\mathbf{d}-\omega^2\left[\mathbf{M}\right]\mathbf{d}=0, \tag{35}$$

where $\mathbf{d}=\{\{A_j\}^T\ \{B_j\}^T\ \{C_j\}^T\}$, $j=1,2,...,N$; $\left[\mathbf{M}\right]$, $\left[\mathbf{K_L}\right]$, $\left[\mathbf{K_{NL1}}\right]$ and $\left[\mathbf{K_{NL2}}\right]$ are the mass matrix, linear stiffness matrix and nonlinear stiffness matrices, respectively. $\left[\mathbf{K_{NL1}}\right]$ is a linear function of $\mathbf{d}$ while $\left[\mathbf{K_{NL2}}\right]$ is a quadratic function of $\mathbf{d}$.

For the analysis of a linear vibration problem, the governing equation (35) is reduced to the following form as

$$\left[\mathbf{K}_{\mathrm{L}}\right]\mathbf{d}-\omega^{2}\left[\mathbf{M}\right]\mathbf{d}=0. \tag{36}$$

Note, the vibrational amplitudes of the unsymmetric double-layer LTCSB in both negative and positive cycles are different, due to the bending–extension coupling effects. Therefore, the nonlinear vibration of the unsymmetric double-layer LTCSB cannot be directly solved using the conventional iterative method [48]. However, the nonlinear free vibration of unsymmetric double-layer LTCSB can be analyzed using a new iterative method proposed by Ke et al. [47], which is developed based on the principle of energy balance at both positive and negative deflection cycles. The computational steps of this method are described as followings:

1. The linear eigenvalue and eigenvector of Eq. (36) are determined, and then eigenvector is normalized with respect to $W_{\max}$, which is assumed as a positive maximum amplitude.

2. Using the eigenvector obtained in step 1 to calculate [K_{NL1}] and [K_{NL2}] and update Eq. (35), which is then used to compute new eigenvalue and eigenvector.

3. Normalizing the new eigenvector again and repeating step 2 until the relative error in two consecutive iterations is less than 0.1%. Then, the iterative outcome is the frequency ω_1 for the positive deflection cycle. The maximum energy $Q^{+}{}_{\max}=Q^{+}{}_{linear}+Q^{+}{}_{nonlinear}$ of the positive deflection cycle is calculated using Eqs. (23) and (24).

4. With a given negative amplitude $W_{\min}$, the energy $Q^{-}{}_{\max}$ in negative deflection cycle is calculated by repeating steps 1-3, and the frequency ω_2 for the negative deflection cycle is obtained until $Q^{-}{}_{\max}=Q^{+}{}_{\max}$.

After obtaining the nonlinear frequencies ω_1 and ω_2 from the above computational steps, the associated periods T_1 and T_2 of two half-cycles are expressed as $T_1=\pi/\omega_1$ and $T_2=\pi/\omega_2$, respectively. Finally, the nonlinear frequency of the unsymmetric double-layer LTCSB is determined by

$$\omega_{nl}=2\pi/\left(T_1+T_2\right)=2\omega_1\omega_2/\left(\omega_1+\omega_2\right). \tag{37}$$

Similarly, the nonlinear frequencies of double-layer LTCSBs for cases I and IV-VI are obtained using the above computational steps. All elements of matrices in the governing equations are given in Appendix A. The dimensionless forms of corresponding coefficients for cases II, III and cases I, IV-VI are given in Appendix B and Appendix C, respectively.

4. Results and discussions

In this section, we study the nonlinear vibration of double-layer LTCSBs with unsymmetric cores or sheets for six different cases I-VI. In case I, the effects to the nonlinear vibration of LTCSBs given rise by the variation of the material properties in two layers are studied. Three material combinations Al_2O_3-Al_2O_3, Al_2O_3-ZrO_2 and Al_2O_3-Al are considered. In case II-VI, the variation of the structural geometry in two layers is studied. Only Al_2O_3 is applied in two layers of cases II-VI. The specific geometry parameters and material properties of double-layer LTCSBs for these six cases are given in Tables 1 and 2.

4.1 Comparison and convergence studies

To verify the present theoretical model, the FEM simulation using the Abaqus software is carried out to compute natural frequency of double-layer LTCSBs. As shown in Fig. 4, the element types of three sheets and struts in the FEM are 4-node shell element with reduced integration (S4R) and 3-node beam element (B32), respectively. In one unit cell, the number of elements for each strut is 10, while the number of elements on each side of the sheet is 12. The natural frequencies of double-layer LTCSBs are obtained using a frequency extraction procedure based on the Lanczos method.

The analytical model developed in this paper is also applicable to analyze the symmetric double-layer LTCSB [40]. Table 3 shows the convergence procedure of the present theoretical model in the prediction of the fundamental frequencies of symmetric double-layer LTCSBs under H-H, C-H and C-C boundary conditions. The geometry parameters and material properties of double-layer LTCSB are: $\alpha = \pi / 4$, $h = 1$ mm, $h_c = 15$ mm, $r_c = 1$mm, $L = 1.6970$ m, $B = 0.1697$ m, $E = 210$ GPa and $\rho = 7930$ kg/m^3. By increasing the total number of polynomial terms N (up to $N = 7$), the analytical model results are gradually convergent to the FEM results and the results given by Li et al. [40]. Therefore, $N = 7$ is selected in the following analysis.

Table 4 gives first three frequencies of Al_2O_3-ZrO_2 double-layer LTCSB with 80 unit-cells for case I. The theoretical and FEM results of the first three frequencies are in good agreement, which approves the accuracy of the present analytical model.

4.2 Nonlinear vibration analysis

Fig. 5 shows the normalized nonlinear frequency vs the vibration amplitude curves of double-layer LTCSBs for case I under three boundary conditions, e.g., H-H, C-H and C-C. It was found that the curves

of H-H and C-H Al_2O_3-ZrO_2 and Al_2O_3-Al double-layer LTCSBs are unsymmetric due to the bending-extension coupling effect. However, the curves of Al_2O_3-Al_2O_3 LTCSBs and C-C LTCSBs are symmetric with respect to the frequency ratio axis. That is because the C-C boundary condition can largely absorb the bending–extension coupling effect. Furthermore, the H-H Al_2O_3-Al LTCSBs exhibit the softening-spring nonlinearity at small amplitudes, i.e., $\omega_{nl}/\omega_l < 1$, but this effect is not observed at small amplitudes in the H-H Al_2O_3-ZrO_2 LTCSBs. This is because that the difference of material properties in Al_2O_3-Al system is greater than that in Al_2O_3-ZrO_2 system. The similar unsymmetrical phenomenon and softening-spring nonlinearity had been reported to occur in FGM beams [49], two-layer beam [50] and asymmetric laminated beams and laminated cylindrical shell [51, 52, 53].

Fig. 6 illustrates the nonlinear frequency ratio vs the vibration amplitude curves of double-layer LTCSBs for case II. Obviously, the curves of C-C LTCSBs and the curves with $h_{bs}/h_{ts}=1$ are symmetric because the bending–extension coupling is zero for these two problems. However, the curves of H-H and C-H LTCSBs with $h_{bs}/h_{ts} \neq 1$ are unsymmetric, and the asymmetry becomes more obvious for the larger thickness ratio. Specially, the curve of H-H beam with a large thickness ratio ($h_{bs}/h_{ts}=5$) also exhibits the softening-spring nonlinearity at small amplitudes but it disappears when the vibration amplitude increases.

Fig. 7 presents the nonlinear frequency ratio vs vibration amplitude curves of double-layer LTCSBs for case III. The curves of H-H and C-H LTCSBs with $h_{bc}/h_{tc} \neq 1$ is unsymmetric, but no softening-spring nonlinearity is observed. That is because the geometry asymmetry of lattice truss cores has little influence on the bending–extension coupling effect, and it can only affect the asymmetry of the curves. However, it does not result in a softening-spring nonlinearity.

Fig. 8 shows the nonlinear frequency ratio vs vibration amplitude curves of double-layer LTCSBs for case IV. It is clearly seen that all curves for H-H, C-H and C-C LTCSBs show the symmetry and hardening-spring nonlinearity. In this case, the bending–extension coupling effect $\bar{B}_{11}$ is zero because only shear deformation is considered at lattice truss cores. In other words, the variation of the length of unit cells in two cores have no contribution on the bending-extension coupling effect. Note, the results for cases V and VI arrive similar conclusions with those for case IV but are not discussed herein for the sake of brevity.

In cases I and II, we found that the softening-spring nonlinearity occurs in H-H double-layer LTCSBs when the material properties or the structural geometry of each layer have a strong asymmetry with respect to the midplane. Under such scenarios, a strong bending–extension coupling effect will be produced in the double-layer LTCSBs. In the next analysis, we will study the combined effect of cases I and II on the softening-spring nonlinearity. Since the C-C boundary condition does not result in the unsymmetric curves for the nonlinear frequency ratio vs amplitude and the softening-spring nonlinearity, only the H-H and C-H double-layer LTCSBs are considered in the following example.

Fig. 9 shows the combined effects on the nonlinear frequency ratio vs vibration amplitude curves of double-layer LTCSBs. We choose the Al_2O_3-Al material system and geometry parameters in case II for the double layers. Only h_{bs} / h_{ts} is allowed to change in the analysis. As expected, the softening-spring nonlinearity is strengthened remarkably with the increase of h_{bs} / h_{ts} from 1 to 2. Interestingly, for a large ratio of h_{bs} / h_{ts} = 6, the softening-spring nonlinearity also occurs in C-H double-layer LTCSBs. These results are implied that the combined effect can increase the bending–extension coupling effect, which in turn leads to a stronger softening-spring nonlinearity than that in a single unsymmetric case.

5. Conclusions

This paper studies the nonlinear vibration of unsymmetric double-layer LTCSBs using two analytical models developed based on Timoshenko beam theory, von Kármán nonlinear theory and Allen model. The Ritz method is employed to obtain the nonlinear vibration frequencies of double-layer LTCSBs with different boundary conditions. The effect of different asymmetries in double-layer LTCSB on the nonlinear vibration behavior is discussed in detail. It was found that:

(1) The nonlinear frequency ratio vs amplitude curves of symmetric double-layer LTCSBs and C-C unsymmetric double-layer LTCSBs are symmetric and exhibit the hardening-spring nonlinearity.

(2) The softening-spring nonlinearity only occurs in cases I and II for H-H double-layer LTCSBs when the material properties or structural geometry of each layer have a strong asymmetry about the midplane. The reason is that it exhibits a strong bending–extension coupling effect in these cases.

(3) The asymmetry in case III may induce obvious unsymmetric curves for double-layer LTCSBs under H-H and C-H boundary conditions, but this does not happen to the cases IV-VI. That is because the asymmetry of unit cells in two cores for cases IV-VI has no contribution to the bending–extension coupling effect.

(4) The combined effect of cases I and II can strengthen the bending–extension coupling effect, and lead to the softening-spring nonlinearity in both H-H and C-H double-layer LTCSBs.

Acknowledgments

This work is funded by the National Natural Science Foundation of China (Nos. 11725207, 11902217, 12011530056 and 12021002).

Appendix A

Rewrite trial functions in Eqs. (31)-(33) as the following form

$$U(\xi)=\sum_{j=1}^{N}A_j\Xi_{1j}\,,\ W(\xi)=\sum_{j=1}^{N}B_j\Xi_{1j}\,,\ \varphi(\xi)=\sum_{j=1}^{N}C_j\Xi_{2j}\,.$$

The elements of linear stiffness matrix $[\mathbf{K}_{\mathbf{L}}]_{3N\times 3N}$ are

$$[\mathbf{K}_{\mathbf{L}}]_{(k,j)}=\int_0^1 k_1\frac{\mathrm{d}\Xi_{1j}}{\mathrm{d}\xi}\frac{\mathrm{d}\Xi_{1k}}{\mathrm{d}\xi}\mathrm{d}\xi\,,\ [\mathbf{K}_{\mathbf{L}}]_{(k,j+N)}=\frac{1}{2}\int_0^1 k_7\frac{\mathrm{d}^2\Xi_{1j}}{\mathrm{d}\xi^2}\frac{\mathrm{d}\Xi_{1k}}{\mathrm{d}\xi}\mathrm{d}\xi\,,$$

$$[\mathbf{K}_{\mathbf{L}}]_{(k,j+2N)}=\frac{1}{2}\int_0^1 k_3\frac{\mathrm{d}\Xi_{2j}}{\mathrm{d}\xi}\frac{\mathrm{d}\Xi_{1k}}{\mathrm{d}\xi}\mathrm{d}\xi\,,\ [\mathbf{K}_{\mathbf{L}}]_{(k+N,j)}=\frac{1}{2}\int_0^1 k_7\frac{\mathrm{d}^2\Xi_{1k}}{\mathrm{d}\xi^2}\frac{\mathrm{d}\Xi_{1j}}{\mathrm{d}\xi}\mathrm{d}\xi\,,$$

$$[\mathbf{K}_{\mathbf{L}}]_{(k+N,j+N)}=\int_0^1\left(k_4\frac{\mathrm{d}^2\Xi_{1k}}{\mathrm{d}\xi^2}\frac{\mathrm{d}^2\Xi_{1j}}{\mathrm{d}\xi^2}+k_5\frac{\mathrm{d}\Xi_{1k}}{\mathrm{d}\xi}\frac{\mathrm{d}\Xi_{1j}}{\mathrm{d}\xi}\right)\mathrm{d}\xi\,,$$

$$[\mathbf{K}_{\mathbf{L}}]_{(k+N,j+2N)}=\frac{1}{2}\int_0^1\left(k_6\frac{\mathrm{d}^2\Xi_{1k}}{\mathrm{d}\xi^2}\frac{\mathrm{d}\Xi_{2j}}{\mathrm{d}\xi}-k_{12}\Xi_{2j}\frac{\mathrm{d}\Xi_{1k}}{\mathrm{d}\xi}\right)\mathrm{d}\xi\,,$$

$$[\mathbf{K}_{\mathbf{L}}]_{(k+2N,j)}=\frac{1}{2}\int_0^1 k_3\frac{\mathrm{d}\Xi_{1j}}{\mathrm{d}\xi}\frac{\mathrm{d}\Xi_{2k}}{\mathrm{d}\xi}\mathrm{d}\xi\,,\ [\mathbf{K}_{\mathbf{L}}]_{(k+2N,j+N)}=\frac{1}{2}\int_0^1\left(k_6\frac{\mathrm{d}^2\Xi_{1j}}{\mathrm{d}\xi^2}\frac{\mathrm{d}\Xi_{2k}}{\mathrm{d}\xi}-k_{12}\Xi_{2k}\frac{\mathrm{d}\Xi_{1j}}{\mathrm{d}\xi}\right)\mathrm{d}\xi\,,$$

$$[\mathbf{K}_{\mathbf{L}}]_{(k+2N,j+2N)}=\int_0^1\left(k_2\frac{\mathrm{d}\Xi_{2k}}{\mathrm{d}\xi}\frac{\mathrm{d}\Xi_{2j}}{\mathrm{d}\xi}+k_{13}\Xi_{2k}\Xi_{2j}\right)\mathrm{d}\xi\,.$$

The elements of nonlinear stiffness matrix $[\mathbf{K}_{\mathbf{NL1}}]_{3N\times 3N}$ are

$$[\mathbf{K}_{\mathbf{NL1}}]_{(k,j+N)}=\frac{1}{2}\int_0^1 k_9\frac{\mathrm{d}W}{\mathrm{d}\xi}\frac{\mathrm{d}\Xi_{1j}}{\mathrm{d}\xi}\frac{\mathrm{d}\Xi_{1k}}{\mathrm{d}\xi}\mathrm{d}\xi\,,\ [\mathbf{K}_{\mathbf{NL1}}]_{(k+N,j)}=\int_0^1 k_9\frac{\mathrm{d}W}{\mathrm{d}\xi}\frac{\mathrm{d}\Xi_{1j}}{\mathrm{d}\xi}\frac{\mathrm{d}\Xi_{1k}}{\mathrm{d}\xi}\mathrm{d}\xi\,,$$

$$[\mathbf{K}_{\mathbf{NL1}}]_{(k+N,j+N)}=\frac{1}{2}\int_0^1 k_{11}\left(\frac{\mathrm{d}W}{\mathrm{d}\xi}\frac{\mathrm{d}\Xi_{1j}}{\mathrm{d}\xi}\frac{\mathrm{d}^2\Xi_{1k}}{\mathrm{d}\xi^2}+\frac{\mathrm{d}^2W}{\mathrm{d}\xi^2}\frac{\mathrm{d}\Xi_{1j}}{\mathrm{d}\xi}\frac{\mathrm{d}\Xi_{1k}}{\mathrm{d}\xi}+\frac{\mathrm{d}W}{\mathrm{d}\xi}\frac{\mathrm{d}\Xi_{1k}}{\mathrm{d}\xi}\frac{\mathrm{d}^2\Xi_{1j}}{\mathrm{d}\xi^2}\right)\mathrm{d}\xi\,,$$

$$[\mathbf{K_{NL1}}]_{(k+N,j+2N)}=\int_0^1 k_{10}\frac{\mathrm{d}W}{\mathrm{d}\xi}\frac{\mathrm{d}\Xi_{2j}}{\mathrm{d}\xi}\frac{\mathrm{d}\Xi_{1k}}{\mathrm{d}\xi}\mathrm{d}\xi,\ [\mathbf{K_{NL1}}]_{(k+2N,j+N)}=\frac{1}{2}\int_0^1 k_{10}\frac{\mathrm{d}W}{\mathrm{d}\xi}\frac{\mathrm{d}\Xi_{1j}}{\mathrm{d}\xi}\frac{\mathrm{d}\Xi_{2k}}{\mathrm{d}\xi}\mathrm{d}\xi.$$

The elements of nonlinear stiffness matrix $[\mathbf{K_{NL2}}]_{3N\times 3N}$ is

$$[\mathbf{K_{NL2}}]_{(k+N,j+N)}=\int_0^1 k_8\left(\frac{\mathrm{d}W}{\mathrm{d}\xi}\right)^2\frac{\mathrm{d}\Xi_{1j}}{\mathrm{d}\xi}\frac{\mathrm{d}\Xi_{1k}}{\mathrm{d}\xi}\mathrm{d}\xi.$$

The elements of mass matrix $[\mathbf{M}]_{3N\times 3N}$ are

$$[\mathbf{M}]_{(k,j)}=\int_0^1 m_1\Xi_{1j}\Xi_{1k}\mathrm{d}\xi,\ [\mathbf{M}]_{(k,j+N)}=\frac{1}{2}\int_0^1 m_5\frac{\mathrm{d}\Xi_{1j}}{\mathrm{d}\xi}\Xi_{1k}\mathrm{d}\xi,$$

$$[\mathbf{M}]_{(k,j+2N)}=\frac{1}{2}\int_0^1 m_2\Xi_{2j}\Xi_{1k}\mathrm{d}\xi,\ [\mathbf{M}]_{(k+N,j)}=\frac{1}{2}\int_0^1 m_5\frac{\mathrm{d}\Xi_{1k}}{\mathrm{d}\xi}\Xi_{1j}\mathrm{d}\xi,$$

$$[\mathbf{M}]_{(k+N,j+N)}=\int_0^1\left(m_1\Xi_{1j}\Xi_{1k}+m_3\frac{\mathrm{d}\Xi_{1j}}{\mathrm{d}\xi}\frac{\mathrm{d}\Xi_{1k}}{\mathrm{d}\xi}\right)\mathrm{d}\xi,\ [\mathbf{M}]_{(k+N,j+2N)}=\frac{1}{2}\int_0^1 m_4\Xi_{2j}\frac{\mathrm{d}\Xi_{1k}}{\mathrm{d}\xi}\mathrm{d}\xi,$$

$$[\mathbf{M}]_{(k+2N,j)}=\frac{1}{2}\int_0^1 m_2\Xi_{2k}\Xi_{1j}\mathrm{d}\xi,\ [\mathbf{M}]_{(k+2N,j+N)}=\frac{1}{2}\int_0^1 m_4\Xi_{2k}\frac{\mathrm{d}\Xi_{1j}}{\mathrm{d}\xi}\mathrm{d}\xi,$$

$$[\mathbf{M}]_{(k+2N,j+2N)}=\int_0^1 m_6\Xi_{2k}\Xi_{2j}\mathrm{d}\xi,$$

where $j,k=1,2,...,N$.

The coefficients of elements in stiffness and mass matrices are

$$k_1=\bar{A}_{11},\ k_2=\bar{A}_{13},\ k_3=-2\bar{A}_{12},k_4=\zeta_2{}^2\left(\bar{A}_{13}-2\bar{B}_{12}+\bar{D}_{11}\right),\ k_5=\bar{A}_{00},$$

$$k_6=2\zeta_2\left(\bar{B}_{12}-\bar{A}_{13}\right),\ k_7=-2\zeta_2\left(\bar{B}_{11}-\bar{A}_{12}\right),\ k_8=\frac{\zeta_2{}^2}{2}\bar{A}_{11},\ k_9=\zeta_2\bar{A}_{11},$$

$$k_{10}=-\zeta_2\bar{A}_{12},\ k_{11}=-\zeta_2{}^2\left(\bar{B}_{11}-\bar{A}_{12}\right),\ k_{12}=\frac{2}{\zeta_2}\bar{A}_{00},\ k_{13}=\frac{1}{\zeta_2{}^2}\bar{A}_{00};$$

$$m_1=\bar{L}_{11},\ m_2=-2\left(\bar{L}_{13}+\bar{L}_{23}\right),\ m_3=\zeta_2{}^2\left(\bar{L}_{12}-2\bar{L}_{22}+\bar{L}_{32}\right),\ m_4=2\zeta_2\left(\bar{L}_{25}-\bar{L}_{12}\right),$$

$$m_5=-2\zeta_2\left(\bar{L}_{21}-\bar{L}_{13}\right),\ m_6=\bar{L}_{12}-2\bar{L}_{24}+\bar{L}_{31}.$$

Appendix B

The dimensionless corresponding coefficients in Appendix A for cases II and III are

$$\bar{A}_{00}=\bar{S}_{tc}+\bar{S}_{bc};\ \bar{A}_{11}=\bar{A}_{ts}+\bar{A}_{ms}+\bar{A}_{bs},\ \bar{A}_{12}=\left(\zeta_3\bar{A}_{ts}+\zeta_4\bar{A}_{ms}-\zeta_5\bar{A}_{bs}\right),$$

$\bar{A}_{13} = \zeta_3{}^2\bar{A}_{ts} + \zeta_4{}^2\bar{A}_{ms} + \zeta_5{}^2\bar{A}_{bs}$; $\bar{B}_{11} = \bar{B}_{ts} + \bar{B}_{ms} + \bar{B}_{bs}$, $\bar{B}_{12} = \zeta_3\bar{B}_{ts} + \zeta_4\bar{B}_{ms} - \zeta_5\bar{B}_{bs}$;

$\bar{D}_{11} = \bar{D}_{ts} + \bar{D}_{ms} + \bar{D}_{bs}$;

$\bar{L}_{11} = \bar{I}_{ts}^0 + \bar{I}_{tc}^0 + \bar{I}_{ms}^0 + \bar{I}_{bc}^0 + \bar{I}_{bs}^0$, $\bar{L}_{12} = \zeta_3{}^2\bar{I}_{ts}^0 + \zeta_1{}^2\bar{I}_{tc}^0 + \zeta_4{}^2\bar{I}_{ms}^0 + \zeta_5{}^2\bar{I}_{bs}^0$, $\bar{L}_{13} = \zeta_3\bar{I}_{ts}^0 - \zeta_1\bar{I}_{tc}^0 + \zeta_4\bar{I}_{ms}^0 - \zeta_5\bar{I}_{bs}^0$;

$\bar{L}_{21} = \bar{I}_{ts}^1 + \bar{I}_{ms}^1 + \bar{I}_{bs}^1$, $\bar{L}_{22} = \zeta_3\bar{I}_{ts}^1 + \zeta_4\bar{I}_{ms}^1 + \zeta_5\bar{I}_{bs}^1$, $\bar{L}_{23} = \bar{I}_{bc}^1 + \bar{I}_{tc}^1$, $\bar{L}_{24} = \zeta_1\bar{I}_{tc}^1$,

$\bar{L}_{25} = \zeta_3\bar{I}_{ts}^1 + \zeta_1\bar{I}_{tc}^1 + \zeta_4\bar{I}_{ms}^1 - \zeta_5\bar{I}_{bs}^1$; $\bar{L}_{31} = \bar{I}_{tc}^2 + \bar{I}_{bc}^2$, $\bar{L}_{32} = \bar{I}_{ts}^2 + \bar{I}_{ms}^2 + \bar{I}_{bs}^2$.

Appendix C

The corresponding dimensionless coefficients for cases I and IV-VI are

$\bar{A}_{00} = \bar{S}_{bc} + \bar{S}_{tc}$; $\bar{A}_{11} = \bar{A}_{ts} + \bar{A}_{ms} + \bar{A}_{bs}$, $\bar{A}_{12} = \zeta_1\bar{A}_{ts} - \zeta_1\bar{A}_{bs}$, $\bar{A}_{13} = \zeta_1{}^2\bar{A}_{ts} + \zeta_1{}^2\bar{A}_{bs}$;

$\bar{B}_{11} = \bar{B}_{ts} + \bar{B}_{bs}$, $\bar{B}_{12} = \zeta_1\bar{B}_{ts} - \zeta_1\bar{B}_{bs}$; $\bar{D}_{11} = \bar{D}_{ts} + \bar{D}_{ms} + \bar{D}_{bs}$;

$\bar{L}_{11} = \bar{I}_{ts}^0 + \bar{I}_{tc}^0 + \bar{I}_{ms}^0 + \bar{I}_{bc}^0 + \bar{I}_{bs}^0$, $\bar{L}_{12} = \zeta_1{}^2\bar{I}_{ts}^0 + \frac{\zeta_3{}^2}{4}\bar{I}_{tc}^0 + \frac{\zeta_3{}^2}{4}\bar{I}_{bc}^0 + \zeta_1{}^2\bar{I}_{bs}^0$,

$\bar{L}_{13} = \zeta_1\bar{I}_{ts}^0 - \frac{\zeta_3}{2}\bar{I}_{tc}^0 - \zeta_1\bar{I}_{bs}^0 + \frac{\zeta_3}{2}\bar{I}_{bc}^0$;

$\bar{L}_{21} = \bar{I}_{ts}^1 + \bar{I}_{bs}^1$, $\bar{L}_{22} = \zeta_1\bar{I}_{ts}^1 - \zeta_1\bar{I}_{bs}^1$, $\bar{L}_{23} = \bar{I}_{bc}^1 + \bar{I}_{tc}^1$, $\bar{L}_{24} = \frac{\zeta_3\bar{I}_{tc}^1 - \zeta_3\bar{I}_{bc}^1}{2}$,

$\bar{L}_{25} = \zeta_1\bar{I}_{ts}^1 + \zeta_3\bar{I}_{tc}^1 - \zeta_3\bar{I}_{bc}^1 - \zeta_1\bar{I}_{bs}^1$;

$\bar{L}_{31} = \bar{I}_{tc}^2 + \bar{I}_{bc}^2$, $\bar{L}_{32} = \bar{I}_{ts}^2 + \bar{I}_{ms}^2 + \bar{I}_{bs}^2$;

where

$$\zeta_1 = \frac{h_c}{H}, \zeta_2 = \frac{H}{L}, \zeta_3 = \frac{h}{H},\ \bar{I}_{bc}^i = \frac{\int_{-\frac{H}{2}}^{-\frac{H}{2}+h} \rho_{bc} z^i \mathrm{d}z}{I_{10} H^i}, \bar{I}_{tc}^i = \frac{\int_{\frac{h}{2}}^{\frac{H}{2}-h} \rho_{tc} z^i \mathrm{d}z}{I_{10} H^i},$$

$$\left(\bar{A}_{ts}, \bar{B}_{ts}, \bar{D}_{ts}\right) = \frac{\int_{\frac{H}{2}-h}^{\frac{H}{2}} E_{ts}\left(1, z, z^2\right)\mathrm{d}z}{A_{10}\left(1, H, H^2\right)},\ \left(\bar{A}_{ms}, \bar{B}_{ms}, \bar{D}_{ms}\right) = \frac{\int_{-\frac{h}{2}}^{\frac{h}{2}} E_{ms}\left(1, z, z^2\right)\mathrm{d}z}{A_{10}\left(1, H, H^2\right)},$$

$$\left(\bar{A}_{bs}, \bar{B}_{bs}, \bar{D}_{bs}\right) = \frac{\int_{-\frac{H}{2}}^{-\frac{H}{2}+h} E_{bs}\left(1, z, z^2\right)\mathrm{d}z}{A_{10}\left(1, H, H^2\right)},\ \bar{S}_{tc} = \frac{\int_{\frac{h}{2}}^{\frac{H}{2}-h} G_{tc}\mathrm{d}z}{A_{10}},\ \bar{S}_{bc} = \frac{\int_{-\frac{H}{2}+h}^{-\frac{h}{2}} G_{bc}\mathrm{d}z}{A_{10}},$$

$$\overline{I}_{ts}^{i}=\frac{\int_{\frac{H}{2}-h}^{\frac{H}{2}}\rho_{ts}z^{i}\mathrm{d}z}{I_{10}H^{i}},\ \overline{I}_{ms}^{i}=\frac{\int_{-\frac{h}{2}}^{\frac{h}{2}}\rho_{ms}z^{i}\mathrm{d}z}{I_{10}H^{i}},\overline{I}_{bs}^{i}=\frac{\int_{-\frac{H}{2}}^{-\frac{H}{2}+h}\rho_{bs}z^{i}\mathrm{d}z}{I_{10}H^{i}}.$$

References

[1] L.J. Gibson, M.F. Ashby, Cellular solids: structure and properties. 2nd ed. Cambridge: Cambridge University Press, 1997.

[2] H. Bart-Smith, J.W. Hutchinson, A.G. Evans, Measurement and analysis of the structural performance of cellular metal sandwich construction, Int. J. Mech. Sci. 43 (2001) 1945–1963.

[3] J.G. Li , X.L. An , J.J. Liang , et al. Recent advances in the stereolithographic three-dimensional printing of ceramic cores: Challenges and prospects. J. Mater. Sci. Technol. 117 (2022) 79–98.

[4] H.N.G. Wadley, N.A. Fleck, A.G. Evans, Fabrication and structural performance of periodic cellular metal sandwich structures, Compos. Sci. Technol. 63 (2003) 2331–2343.

[5] V.S. Deshpande, N.A. Fleck, Collapse of truss core sandwich beams in 3-point bending, Int. J. Solids Struct. 38 (2001) 6275–6305.

[6] T.A. Sebaey, E. Mahdi, Crushing behavior of a unit cell of CFRP lattice core for sandwich structures' application, Thin-Walled Struct. 116 (2017) 91–95.

[7] W. Yang, J. Xiong, L.J. Feng, et al. Fabrication and mechanical properties of three-dimensional enhanced lattice truss sandwich structures. J. Sandw. Struct. Mater. 22 (2020) 1594–1611.

[8] L.H. Yang, X. Han, L.J. Feng, Z.B. Chen, G.C. Yu, J. Qu, J.S. Yang, L.Z. Wu, Numerical investigations on blast resistance of sandwich panels with multilayered graded hourglass lattice cores, J. Sandw. Struct. Mater. 22 (2020) 2139–2156.

[9] X. Han, L.H. Yang, G.C. Yu, J. Qu, L.Z. Wu, Blast resistance of multilayer graded lattice sandwich structures, Chinese Journal of Applied Mechanics 35 (2018) 185–190.

[10] K. Finnegan, G. Kooistra, H.N.G. Wadley, V.S. Deshpande, The compressive response of carbon fiber composite pyramidal truss sandwich cores, Int. J. Mater. Res. 98 (2007) 1264–1272.

[11] H.L. Fan, F.H. Meng, W. Yang, Mechanical behaviors and bending effects of carbon fiber reinforced lattice materials, Arch. Appl. Mech. 75 (2006) 635–647.

[12] J. Xiong, L. Ma, S. Pan, L.Z. Wu, J. Papadopoulos, A. Vaziri, Shear and bending performance of carbon fiber composite sandwich panels with pyramidal truss cores, Acta Mater. 60 (2012) 1455–1466.

[13] J. Xiong, L. Ma, L.Z. Wu, J.Y. Liu, A. Vaziri, Mechanical behavior and failure of composite pyramidal truss core sandwich columns, Compos. Pt. B-Eng. 42 (2011) 938–945.

[14] Y.C. Hu, H.J. Bi, G.Y. Ye, Compression behaviors of 3D printed pyramidal lattice truss composite

structures, Compos. Struct. 233 (2020) 111706.

[15] J.H. Lim, K.J. Kang, Mechanical behavior of sandwich panels with tetrahedral and Kagome truss cores fabricated from wires, Int. J. Solids Struct. 43 (2006) 5228–5246.

[16] B. Wang, L.Z. Wu, L. Ma, Q. Wang, S.Y. Du, Mechanical behavior of the sandwich structures with carbon fiber-reinforced pyramidal lattice truss core, Mater. Des. 31 (2010) 2659–2663.

[17] Y.J. Wang, Z.J. Zhang, X.M. Xue, L. Zhang, Free vibration analysis of composite sandwich panels with hierarchical honeycomb sandwich core, Thin-Walled Struct. 145 (2019) 106425.

[18] L.H. Yang, L. Sui, Y.L. Dong, X.Y. Li, F. Zi, Z.X. Zhang, S.J. Yang, L.Z. Wu, Quasi-static and dynamic behavior of sandwich panels with multilayer gradient lattice cores, Compos. Struct. 255 (2020) 112970.

[19] X. Gao, M.M. Zhang, Y.D. Huang, L. Sang, W.B. Hou, Experimental and numerical investigation of thermoplastic honeycomb sandwich structures under bending loading, Thin-Walled Struct. 155 (2020) 106961.

[20] L. Ge, H.Y. Zheng, H.M. Li, B.S. Liu, H.R. Su, D.N. Fang, Compression behavior of a novel sandwich structure with bi-directional corrugated core, Thin-Walled Struct. 161 (2021) 10741.

[21] Z.K. Guo, C.C. Liu, F.M. Li, Vibration analysis of sandwich plates with lattice truss core, Mech. Adv. Mater. Struct. 26 (2019) 424–429.

[22] K. Kohsaka, K. Ushijima, W.J. Cantwell, Study on vibration characteristics of sandwich beam with BCC lattice core, Mater. Sci. Eng. B-Adv. Funct. Solid-State Mater. 264 (2021) 114986.

[23] X.Y. Zhang, H. Zhou, W.H. Shi, F.M. Zeng, H.Z. Zeng, G. Chen, Vibration tests of 3D printed satellite structure made of lattice sandwich panels, AIAA J. 56 (2018) 4213–4217.

[24] Y.Y. Chai, S.J. Du, F.M Li, C.Z. Zhang, Vibration characteristics of simply supported pyramidal lattice sandwich plates on elastic foundation: Theory and experiments, Thin-Walled Struct. 166 (2021) 108116.

[25] J. Lou, L. Ma, L.Z. Wu, Free vibration analysis of simply supported sandwich beams with lattice truss core, Mater. Sci. Eng. B-Adv. Funct. Solid-State Mater. 177 (2012) 1712–1716.

[26] H.G. Allen, Analysis and Design of Structural Sandwich Panels. Oxford: Pergamon Press, 1969.

[27] J. Lou, B. Wang, L. Ma, L.Z. Wu, Free vibration analysis of lattice sandwich beams under several typical boundary conditions, Acta Mech. Solida Sin. 26 (2013) 458–467.

[28] M.H. Xu, Z.P. Qiu, Free vibration analysis and optimization of composite lattice truss core sandwich

beams with interval parameters, Compos. Struct. 106 (2013) 85–95.

[29] Z. Zhao, S.R. Wen, F.M. Li, Vibration analysis of multi-span lattice sandwich beams using the assumed mode method, Compos. Struct. 185 (2018) 716–727.

[30] G. Yao, F.M. Li, Nonlinear primary resonances of lattice sandwich beams with pyramidal truss core and viscoelastic surfaces, Acta Mech. 229 (2018) 4091–4100.

[31] M. Liu, D.Q. Gao, X.Y. Zhang, J. Wei, D.F. Zhu, Nonlinear dynamic responses of beamlike truss based on the equivalent nonlinear beam model, Int. J. Mech. Sci. 194 (2021) 106197.

[32] Y.Y. Chai, F.M. Li, Z.G. Song, C.Z. Zhang, Analysis and active control of nonlinear vibration of composite lattice sandwich plates, Nonlinear Dyn. 102 (2020) 2179–2203.

[33] P. Nampally, A.T. Karttunen, J.N. Reddy, Nonlinear finite element analysis of lattice core sandwich plates, Int. J. Non-Linear Mech. 121 (2020) 103423.

[34] D.H. Li, R.P. Wang, R.L. Qian, Y. Liu, G.H. Qing, Static response and free vibration analysis of the composite sandwich structures with multi-layer cores, Int. J. Mech. Sci. 111 (2016) 101–115.

[35] B.T. Cao, B. Hou, Y.L. Li, H. Zhao, An experimental study on the impact behavior of multilayer sandwich with corrugated cores, Int. J. Solids Struct. 109 (2017) 33–45.

[36] B.T. Cao, B. Hou, H. Zhao, Y.L. Li, J.G. Liu, On the influence of the property gradient on the impact behavior of graded multilayer sandwich with corrugated cores, Int. J. Impact Eng. 113 (2018) 98–105.

[37] G.D. Xu, J.J. Zhai, T. Zeng, Z.H. Wang, S. Cheng, D.N. Fang, Response of composite sandwich beams with graded lattice core, Compos. Struct. 119 (2015) 666–676.

[38] Y. Sun, L.C. Guo, T.S. Wang, S.Y. Zhong, H.Z. Pan, Bending behavior of composite sandwich structures with graded corrugated truss cores, Compos. Struct. 185 (2018) 446–454.

[39] A. Pydah, R.C. Batra, Analytical solution for cylindrical bending of two-layered corrugated and webcore sandwich panels, Thin-Walled Struct. 123 (2018) 509–519.

[40] L. Meng, S.J. Du, F.M. Li, X.J. Jing, Vibration characteristics of novel multilayer sandwich beams: Modelling, analysis and experimental validations, Mech. Syst. Signal Proc. 142 (2020) 106799.

[41] Z.K. Guo, X.D. Yang, W. Zhang, Dynamic analysis, active and passive vibration control of double-layer hourglass lattice truss structures, J. Sandwich Struct. Mater. 22 (2020) 1329–1356.

[42] L.X. Liu, W.Y. Yang, Y.Y. Chai, G.F. Zhai, Vibration and thermal buckling analyses of multi-span composite lattice sandwich beams, Arch. Appl. Mech. 91 (2021) 2601–2616.

[43] Z.K. Guo, G.B. Hu, V. Sorokin, Y. Yang, L.H. Tang, Sound transmission through sandwich plate with

hourglass lattice truss core, J. Sandw. Struct. Mater. 23 (2021) 1902–1928.

[44] S. Kitipornchai, L.L. Ke, J. Yang, Y. Xiang, Nonlinear vibration of edge cracked functionally graded Timoshenko beams, J. Sound Vib. 324 (2009) 962–982.

[45] J.E. Chen, W. Zhang, M. Sun, M.H. Yao, Free vibration and hardening behavior of truss core sandwich beam, Shock Vib. 2016 (2016) 1–13.

[46] K.M. Liew, C.M. Wang, Y. Xiang, S. Kitipornchai, Vibration of Mindlin plates: programming the p-version ritz method, Oxford, Elsevier Science, 1998.

[47] L.L. Ke, J. Yang, S. Kitipornchai, Nonlinear free vibration of functionally graded carbon nanotube-reinforced composite Timoshenko beam, Compos. Struct. 92 (2010) 676–683.

[48] R.K. Gupta, Gunda Jagadish Babu, G. Ranga Janardhan, G. Venkateswara Rao, Relatively simple finite element formulation for the large amplitude free vibrations of uniform beams. Finite Elem. Anal. Des. 45 (2009) 624–631.

[49] L.L. Ke, J. Yang, S. Kitipornchai, An analytical study on the nonlinear vibration of functionally graded beams, Meccanica 45 (2010) 743–752.

[50] N. Hao, L.L. Ke, Softening-spring phenomenon in large amplitude vibration of two-layer bi-material beams, Int. J. Struct. Stab. Dyn. (2022) 2250106. https://doi.org/10.1142/S0219455422501061.

[51] G. Singh, G.V. Rao, Nonlinear oscillations of thick asymmetric cross-ply beams, Acta Mech. 127 (1998) 135–146.

[52] G. Singh, G.V. Rao, N. Iyengar, Analysis of nonlinear vibrations of unsymmetrically laminated composite beam, AIAA J. 29 (1991) 1727–1735.

[53] Mohd. Taha Parvez, A.H. Khan and M. Yaqoob Yasin, On the softening and hardening nonlinear behavior of laminated cylindrical shells. Eng. Struct. 226 (2021) 111339.

Table 1 Geometry parameters of double-layer LTCSB in different cases (L=1.0607 m, B=0.06364 m).

Parameters	Cases I and VI	Case II	Case III	Case IV	Case V
h_{ms}	0.001 m	0.001 m	0.001 m	0.001 m	0.001 m
h_{ts}	0.001 m	0.001 m	0.001 m	0.001 m	0.001 m
h_{bs} / h_{ts}	1	variable	1	1	1
h_{tc}	0.015 m	0.015 m	variable	0.015 m	0.015 m
h_{bc} / h_{tc}	1	1	variable	1	1
H	0.033 m	variable	0.033 m	0.033 m	0.033 m
b_c	0.02121 m	0.02121 m	0.02121 m	0.02121 m	0.02121 m
d_{bc}	0.02121 m	0.02121 m	0.02121 m	variable	0.02121 m
d_{bc} / d_{tc}	1	1	1	variable	1
r_{tc}	0.002 m	0.002 m	0.002 m	0.002 m	0.002 m
r_{bc} / r_{tc}	1	1	1	1	variable

Table 2 Material properties of double-layer LTCSB.

Materials	Elastic modulus (E)	Density (ρ)	Poisson's ratio (v)
Al_2O_3	320 GPa	3800 kg/m^3	0.26
ZrO_2	116 GPa	3657 kg/m^3	0.298
Al	70 GPa	2700 kg/m^3	0.33

Table 3 Convergence and comparison of fundamental frequency (Hz) of double-layer LTCSB with different boundary conditions.

N	H-H	C-H	C-C
3	34.234	47.857	68.635
4	30.896	47.801	68.627
5	30.896	47.752	68.387
6	30.887	47.745	68.359
7	30.887	47.739	68.349
FEM	30.91	46.72	66.80
Li et al. [40]	30.89	-	-

Table 4 First three frequencies (Hz) of Al_2O_3-ZrO_2 double-layer LTCSB with 80 unit-cells for case I.

	H-H		C-H		C-C	
Mode	Present	FEM	Present	FEM	Present	FEM
1	33.27	34.30	48.76	48.59	69.59	67.37
2	123.39	121.38	155.61	150.50	190.45	181.33
3	281.99	264.86	329.92	303.52	387.73	345.08

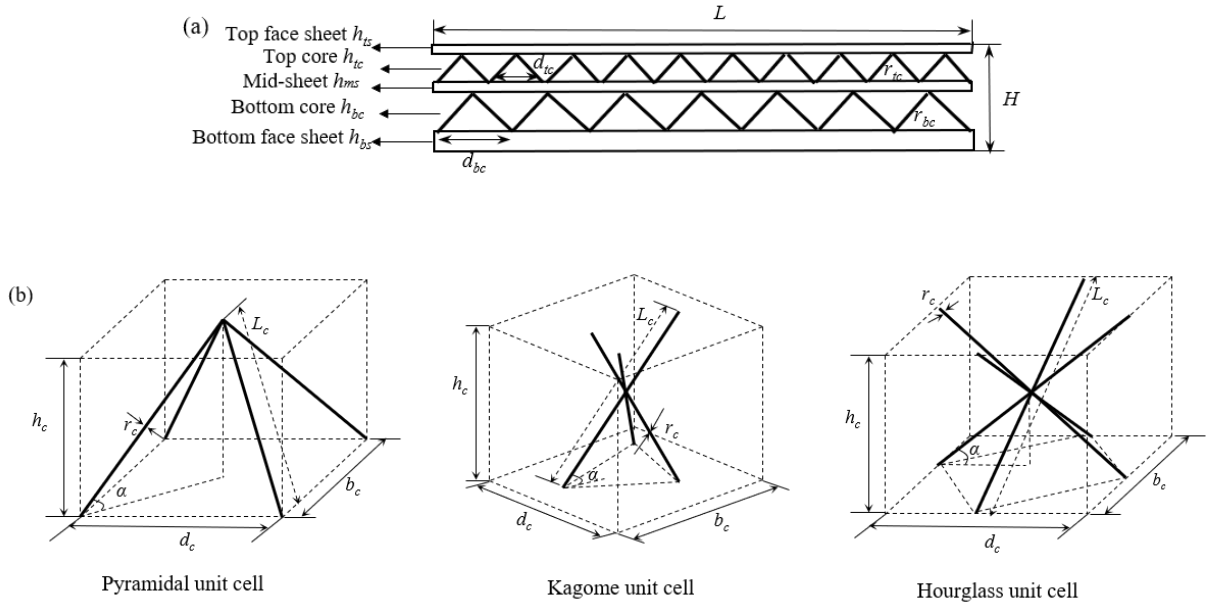

Fig. 1. Sketches of an unsymmetric double-layer LTCSB (a) and different unit cells in the top and bottom cores (b).

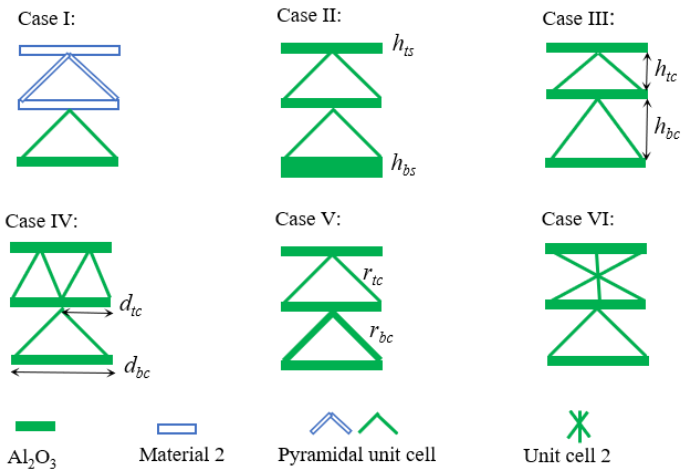

Fig. 2. Short elements along length of double-layer LTCSB for six cases.

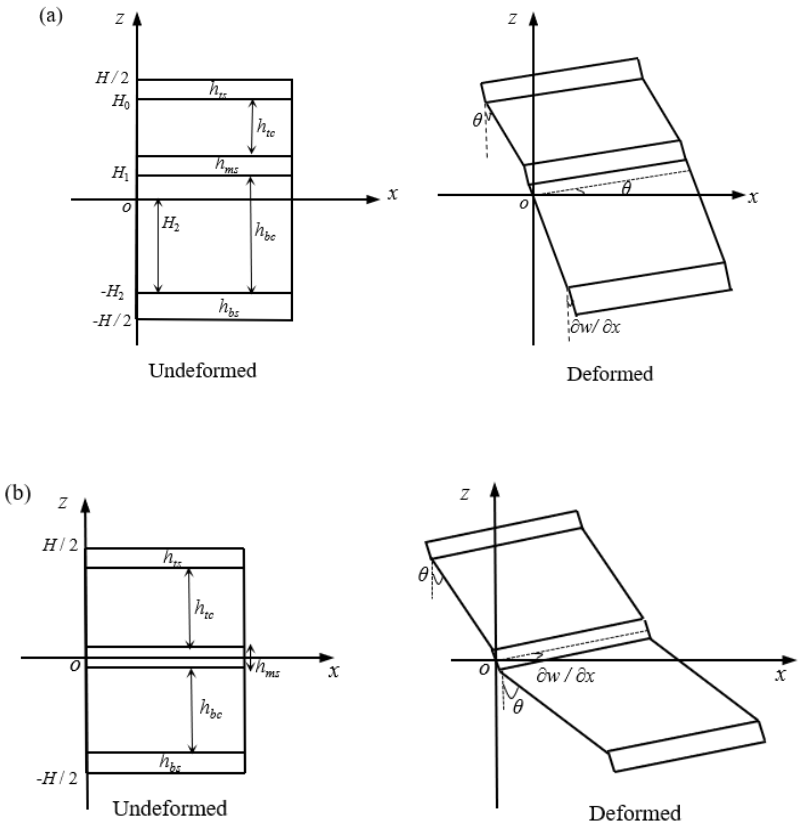

Fig. 3. Undeformed and deformed infinitesimal elements of the double-layer LTCSB in *xz*-plane: (a) the midplane lies in the bottom core layer ($h_{ms} = h_{ts} < h_{bs}$ or $h_{tc} < h_{bc}$), and (b) the midplane lies in the middle position of middle sheet ($h_{ts} = h_{ms} = h_{bs}$ and $h_{tc} = h_{bc}$).

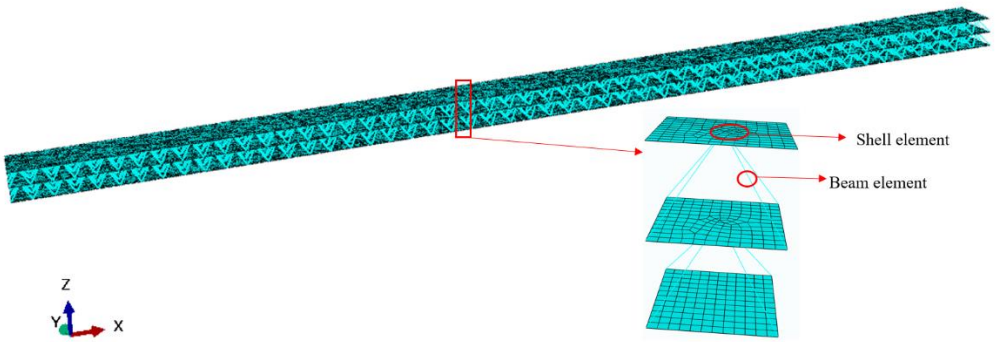

Fig. 4. FEM model and total mesh of the double-layer LTCSB for case I.

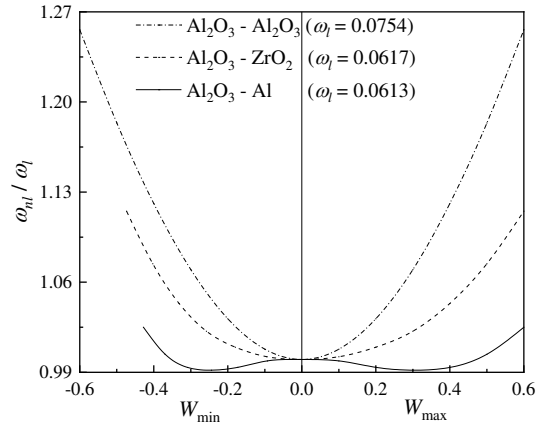

(a)

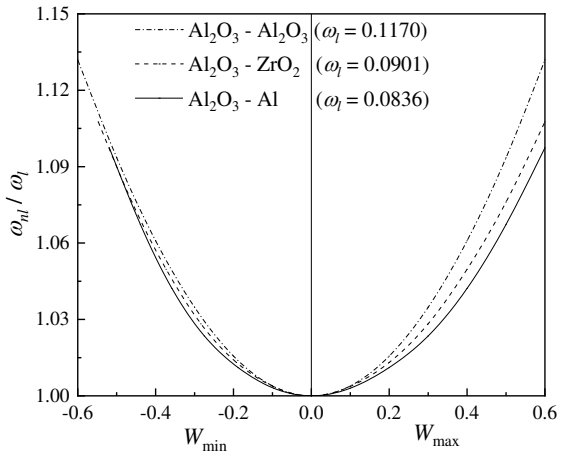

(b)

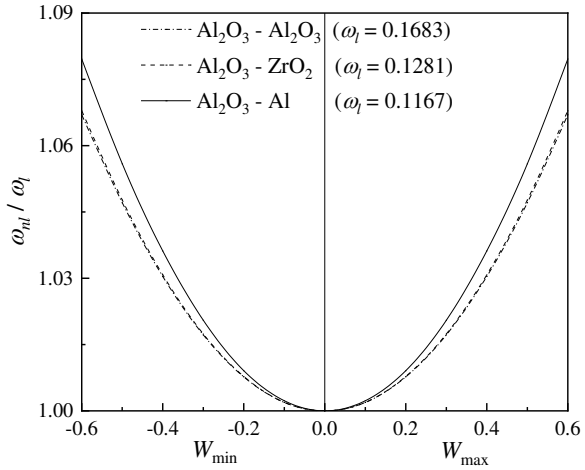

(c)

Fig. 5. The ω_{nl} / ω_l vs amplitude curves of double-layer LTCSB for case I: (a) H-H, (b) C-H and (c) C-C.

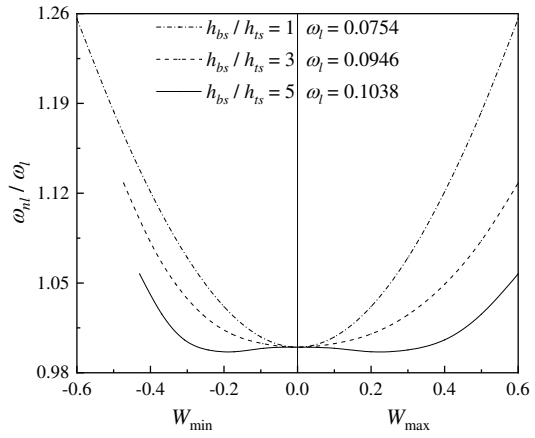

(a)

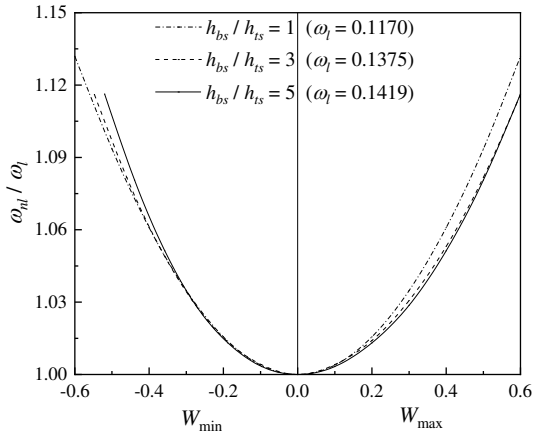

(b)

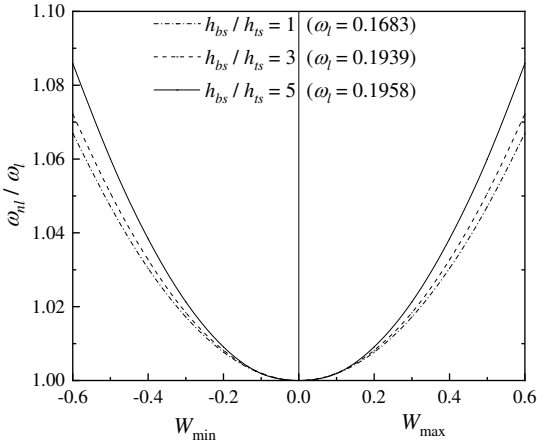

(c)

Fig. 6. The ω_{nl} / ω_l vs amplitude curves of double-layer LTCSB for case II: (a) H-H, (b) C-H and (c) C-C.

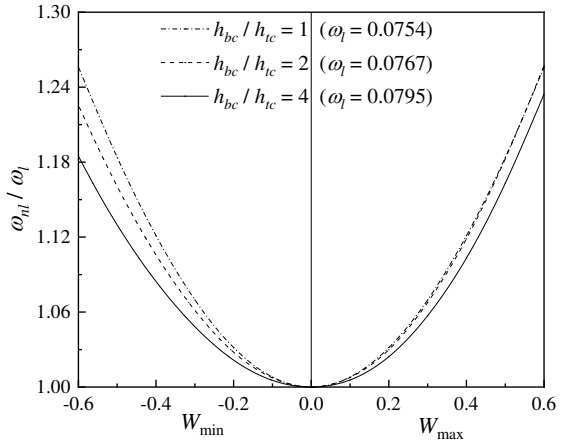

(a)

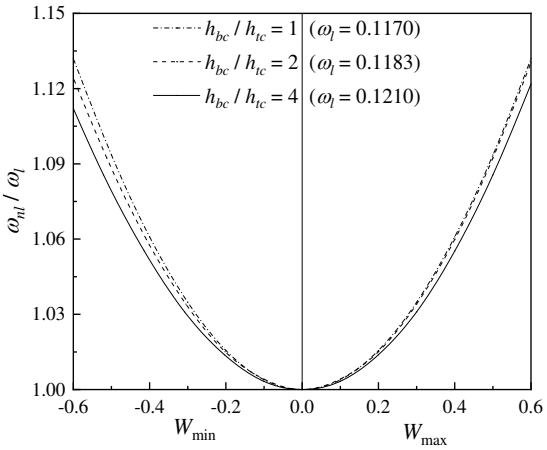

(b)

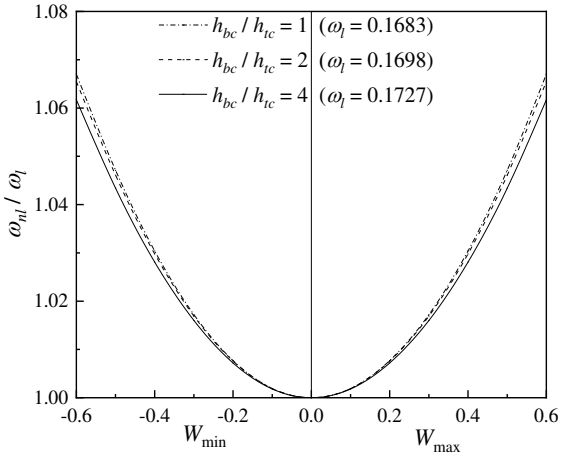

(c)

Fig. 7. The ω_{nl} / ω_l vs amplitude curves of double-layer LTCSB for case III: (a) H-H, (b) C-H and (c) C-C.

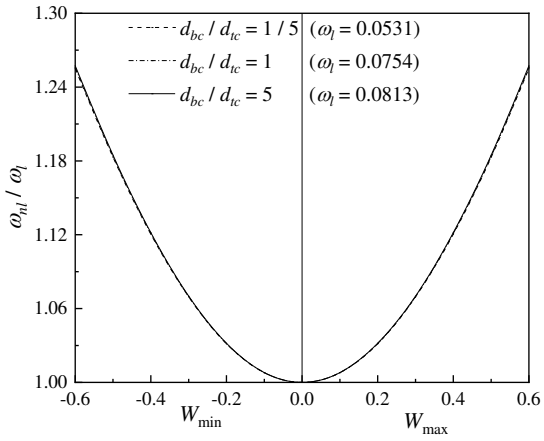

(a)

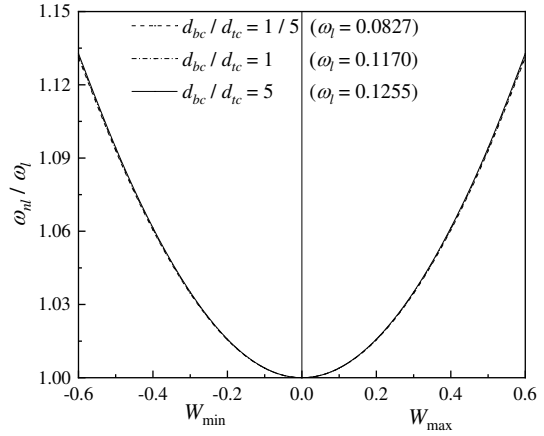

(b)

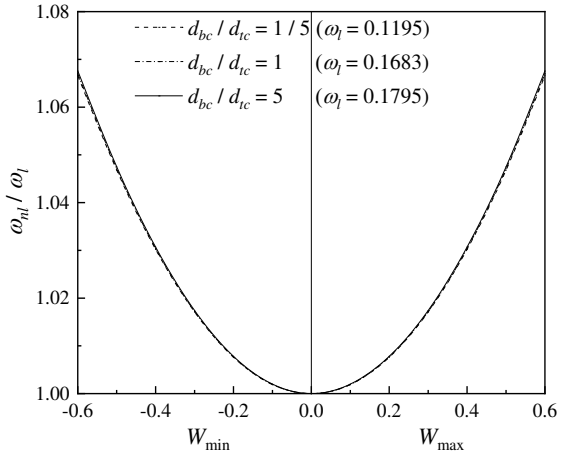

(c)

Fig. 8. The ω_{nl} / ω_l vs amplitude curves of double-layer LTCSB for case IV: (a) H-H, (b) C-H and (c) C-C.

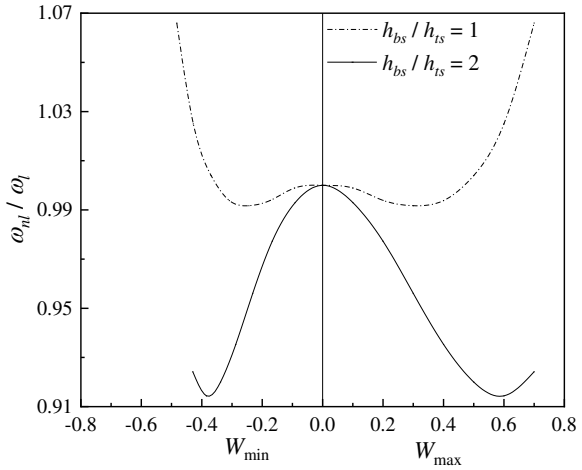

(a)

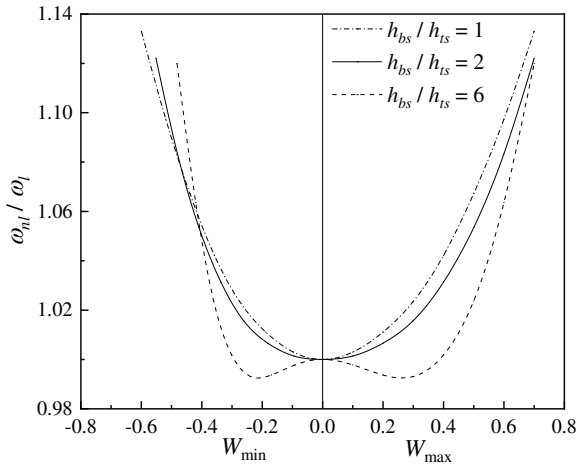

(b)

Fig. 9. Combined effect on the ω_{nl} / ω_l vs amplitude curves of double-layer LTCSB for cases I and II: (a) H-H and (b) C-H.